ELSEVIER

Journal of Nuclear Materials 245 (1997) 191–200

journal of nuclear materials

Oxidation kinetics and microstructure of V–(4–5) wt% Cr–(4–5) wt% Ti alloys exposed to air at 300–650°C

M. Uz [a], K. Natesan [b,*], V.B. Hang [c,1]

[a] *Chemical Engineering Department, Lafayette College, Easton, PA 18042, USA*
[b] *Energy Technology Division, Argonne National Laboratory, Argonne, IL 60439, USA*
[c] *Merck Pharmaceuticals, Technical Operations Division, Rahway, NJ, USA*

Received 26 August 1996; accepted 6 January 1997

Abstract

We conducted a systematic study to determine the effects of time and temperature of air exposure on the oxidation behavior and microstructure of V–4Cr–4Ti and V–5Cr–5Ti alloys. All samples were from 1 mm thick cold-rolled sheets, and each was annealed in vacuum at 1050°C for 1 h prior to high-temperature exposure. Different samples from each alloy were heated in ambient air at 500°C for times ranging from 24 to ≈ 2000 h, and in a thermogravimetric analysis (TGA) apparatus at temperatures ranging from 300 to 650°C. Models describing the oxidation kinetics, oxide type and its thickness, alloy grain size, and depth of oxygen diffusion in the substrate alloy were determined for the two alloys and compared. The results showed that the oxide layers that formed on the surfaces of both alloys in air at 300–650°C are protective, and that the V–5Cr–5Ti alloy is slightly more oxidation-resistant than the V–4Cr–4Ti alloy.

1. Introduction

In general, the alloys of refractory metals of groups VB and VIB have been considered for high-temperature and aerospace applications for the past four decades because of their relatively high melting points and ability to retain strength at elevated temperatures [1–3]. The applications for which refractory metal alloys receive particular attention are the advanced power systems such as the fast breeder, as well as thermonuclear and magnetic fusion reactors [4,5], which are considered to be the principal means to meet future energy needs. The construction and successful operation of these power systems require materials to meet the stringent design criteria, which include operating temperatures of 300–600°C, total stress of 200–750 MPa, total neutron flux of 1.2×10^{19} neutrons m^{-2} s^{-1} [6]. Vanadium-base alloys, together with several other alloys (including Type 316 austenitic stainless steel and HT-9 ferritic steel), are identified as the candidates for such applications. For the first wall and other structural components of the fusion reactors, vanadium-base alloys are reported to be more suitable than the other candidate alloys because of their lower long-term activation, lower irradiation afterheat, lower biological hazard potential and thermal stress factor, better creep resistance, compatibility with coolants such as liquid alkali metals, and better mechanical formability [7–12]. As a result of recent investigations conducted to evaluate and screen the candidate alloys, vanadium alloys nominally containing 4–5 wt% chromium and 4–5 wt% titanium have been identified as the most viable materials for fusion reactor applications because they have the most desirable combinations of the necessary properties mentioned above [13–20].

As is the case for most metals and alloys, a primary deterrent to the use of vanadium-base alloys at elevated temperatures is their relatively high affinity for interstitial impurities, i.e., oxygen, nitrogen, hydrogen and carbon. These impurities are known to increase hardness and strength with an accompanying decrease in ductility and formability. In particular, oxygen (the subject of this pa-

* Corresponding author. Tel.: +1-630 252 5103; fax: +1-630 252 3604; e-mail: ken_natesan@qmgate.anl.gov.

[1] Formerly a student in Chemical Engineering Department, Lafayette College, Easton, PA, USA.

PII S0022-3115(97)00008-1

per) may degrade alloy properties during service through solution in the matrix or formation of oxide particles in the matrix, along the grain boundaries, and/or on the surface of the alloys. Also, the presence of Ti in V-base alloys makes the problems associated with O more of a concern and more complicated. This is because Ti is a stronger oxide former than either V or Cr [21] and is known to trap (or bind) O in solution in refractory metals and alloys [22] and also to act as a scavenger of oxygen [23]. Therefore, a good understanding of the oxidation behavior of the alloys intended for elevated-temperature use is of significant importance.

A number of studies on the oxidation behavior of V [24–28] and various V-base alloys [29–32] have been published. However, no systematic work on ternary V–Cr–Ti alloys has been reported. The present work compares the air-oxidation behaviors of V–4Cr–4Ti and V–5Cr–5Ti alloys in the temperature range of 300–650°C as part of an ongoing project that is assessing the viability of these alloys as structural materials in fusion reactors. From here on in this paper, the V–4Cr–4Ti and V–5Cr–5Ti alloys are referred to as 44 and 55, respectively, and all compositions are stated in percent or parts per million by weight unless otherwise specified.

2. Experimental

The 44 and 55 alloys were obtained as 1 mm thick cold-rolled sheets. Samples with dimensions of about $1 \times 10 \times 20$ mm were cut from each alloy. Before any further treatment or testing, all samples were annealed for 1 h at 1050°C under a pressure of $\approx 10^{-6}$ Torr. The samples were wrapped in tantalum foil to protect them from contamination during this heat treatment process. Samples from each alloy were analyzed for chemical composition before and after annealing, and the results can be seen in Table 1. As seen in the Table the total amount of other impurities in either alloy was $< 0.3\%$, with silicon as the major impurity at $\approx 0.08\%$.

Different samples from the 44 and 55 alloys were heated in air at 500°C for about 24, 250, 600, 1050, and 2100 h to study the effects of time on their oxidation behavior. Samples from each alloy were also heated in a thermogravimetric analysis (TGA) apparatus in air at different temperatures to determine the oxidation kinetics as a function of temperature. The TGA experiments were carried out at 320, 400, 500, 575 and 620°C for the 44 samples, and at 300, 400, 500, 575, and 650°C for the 55 samples. Weight gain was recorded continuously on a strip chart throughout each TGA experiment. All samples were also weighed separately before and after high-temperature exposure to determine the resulting total weight change.

The oxide scales on the samples were identified by X-ray diffraction (XRD) analysis on the surface of several samples, as well as on the oxides scraped from their surfaces. Oxide residues obtained from 44 and 55 alloys exposed to air at 500°C for 2100 h by dissolving away the matrix were analyzed for V, Cr, and Ti by the inductively coupled plasma (ICP) technique. A 900 mL methanol–100 mL bromine–10 g tartaric acid was used for phase extraction with platinum (Pt) wire as the catalyst. Longitudinal and transverse cross-sections of the cold-rolled and thermally treated samples were cut using a diamond wafering blade and metallographically examined by optical microscope and scanning electron microscope (SEM). The metallographic specimens were chemically etched with a solution of lactic–nitric–hydrofluoric acids at a volume ratio of 30–15–5. The grain size of each sample exposed to high temperature (annealed or air-oxidized) was determined by both linear and areal analysis methods according to ASTM Standard E112, and the average of the two was reported as the grain size of each sample. Oxygen diffusion depth (or depth of the hardened layer) of each oxidized sample was estimated from the microhardness profile along its thickness, which was obtained with a Vickers microhardness tester and a load of 25–50 g. Furthermore, the oxygen profiles of several samples were determined by secondary ion mass spectroscopy (SIMS) line-profiles along the thickness to verify the results of the microhardness measurements.

All data in this study were processed and analyzed with a spreadsheet program capable of graphical, statistical, and regression analyses.

Table 1
Chemical composition of the V–4 wt% Cr–4 wt% Ti (44) and V–5 wt% Cr–5 wt% Ti (55) alloys [a]

Alloy	Condition	Composition					
		V (wt%)	Cr (wt%)	Ti (wt%)	O (ppmw)	N (ppmw)	C (ppmw)
44	As-rolled [b]	92.1	3.59	3.97	450	65	330
44	As-annealed [c]	92.7	3.50	3.54	360	73	400
55	As-rolled [b]	91.0	4.72	3.97	440	< 10	300
55	As-annealed [c]	91.0	4.28	4.48	480	74	200

[a] The heat numbers for 44 and 55 alloys are 832665 and 820630, respectively.
[b] Cold-rolled, 1 mm thick sheet.
[c] Annealed at 1050°C for 1 h.

3. Results and discussion

3.1. Oxide scale

The photomicrographs in Fig. 1(top), (bottom) show the oxide scales that formed on the surfaces of, respectively, 44 and 55 alloy sheets during exposure to air for ≈ 2100 h at 500°C. The shape and morphology of the oxides that formed on these samples at temperatures of up to 650°C were similar to those in Fig. 1, with the exception of scale thickness. Examination of the photomicrographs indicates that the oxide layers in both alloys were continuous and tenacious. The tenacity of the oxide was also evidenced by the lack of spalling during handling of the oxidized samples of either alloy. It is also noteworthy from the photomicrographs that the oxide layers were uneven in thickness and appear to be composed of two different layers, i.e., two different oxides. ICP analysis of the residue extracted from the air-oxidized 44 and 55 alloys yielded ≈ 10% Ti–5% Cr, with the balance V. This indicates that some complex oxide of V, Cr, and Ti may be present in these samples in addition to V_2O_5. However, the ICP analysis gives no information on where the oxides are located in the sample, i.e., surface or matrix. On the other hand, XRD analyses of the oxides on the surface of the air-oxidized samples in this study showed that the predominant oxide was V_2O_5. Typical XRD results are shown in Fig. 2(a), (b) for the air-oxidized 44 and 55 alloy samples, respectively. The XRD spectra indicate a weak possibility of a small amount of VO_2, especially in the 55 alloy samples. No oxides of Cr or Ti were detected on the surface, even though Ti is a stronger oxide former than V. Also, partial melting of the surface oxide on a 44 sample heated at ≈ 660°C in air further supported the view that V_2O_5, which has a melting point of about 670°C, is the predominant oxide that formed on these alloys during exposure to air at 300–650°C. These results are consistent with those of Mukherjee and Wach [27] who reported that V_2O_5 is the only oxide that formed on V at 450–600°C and 1 atm (760 Torr) oxygen pressure. However, they also reported VO_2 as the only oxide at a pO_2 of 36 Torr and below in the same temperature range, also on V.

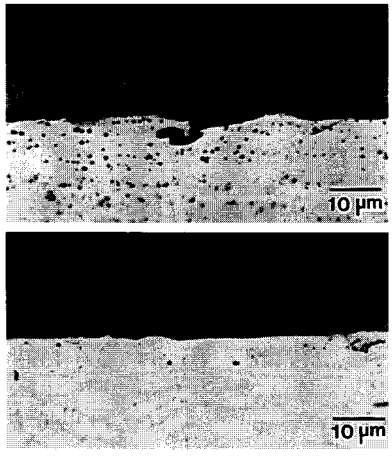

Fig. 1. Optical photomicrographs of oxide scale formed on surface (top) 44 alloy, and (bottom) 55 alloy after exposure to air for ≈ 2100 h at 500°C. As-etched, differential interference contrast.

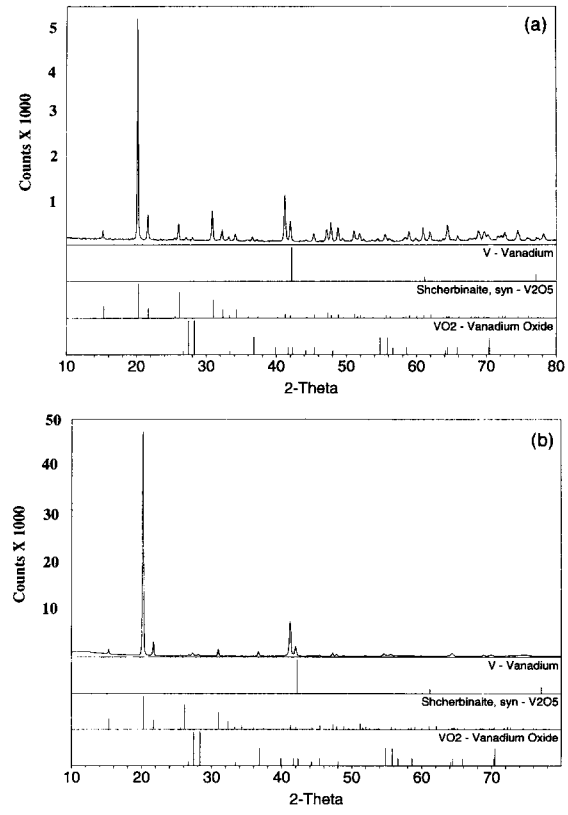

Fig. 2. X-ray diffraction spectra of surface of samples exposed to air: (top) 44 alloy for 120 h at 620°C, and (bottom) 55 alloy for ≈ 100 h at 650°C

3.2. Oxidation models and kinetics

The results of the TGA experiments carried out to determine the oxidation behavior of the 44 and 55 alloys in the temperature range of 300–650°C are tabulated in Table 2, with sample and oxidation temperatures given in columns 1 and 2, respectively. In column 3, the first equation at each temperature represents the oxidation model that best fit the experimental data. The second equation represents the parabolic model and provides a more conservative rate constant (coefficient of time) at that temperature. In the first two equations, w_f and w_p have the units of (mg mm^{-2}), and time t is in hours (h). The third equation in column 3 at each temperature, x with units of mm^2, was obtained by dividing the first equation by the square of

Table 2
Mathematical models describing oxidation behavior of V–4 wt% Cr–4 wt% Ti (44) and V–5 wt% Cr–5 wt% Ti (55) alloys as obtained using data from TGA experiments [a]

Alloy	T (°C)	Oxidation model	R^2
44	350	$w_f^2 = -1.77 \times 10^{-8} + 6.76 \times 10^{-9} t$	0.999
		$w_p^2 = 6.54 \times 10^{-9} t$	0.997
		$x^2 = -1.57 \times 10^{-9} + 6.00 \times 10^{-10} t$	
44	400	$w_f^2 = 1.31 \times 10^{-6} + 1.28 \times 10^{-7} t$	0.999
		$w_p^2 = 1.43 \times 10^{-7} t$	0.984
		$x^2 = 1.16 \times 10^{-7} + 1.14 \times 10^{-8} t$	
44	500	$w_f^2 = 1.17 \times 10^{-5} + 9.82 \times 10^{-7} t$	1.0
		$w_p^2 = 1.08 \times 10^{-6} t$	0.992
		$x^2 = 1.04 \times 10^{-6} + 8.71 \times 10^{-8} t$	
44	575	$w_f^2 = 7.81 \times 10^{-5} + 1.07 \times 10^{-5} t$	1.0
		$w_p^2 = 1.16 \times 10^{-5} t$	0.998
		$x^2 = 6.93 \times 10^{-6} + 9.50 \times 10^{-7} t$	
44	620	$w_f^2 = -5.40 \times 10^{-5} + 2.54 \times 10^{-5} t$	1.0
		$w_p^2 = 2.48 \times 10^{-5} t$	0.998
		$x^2 = -4.79 \times 10^{-6} + 2.25 \times 10^{-6} t$	
55	[b]300		
55	400	$w_f^2 = -3.88 \times 10^{-7} + 4.13 \times 10^{-7} t^{1/2} + 5.23 \times 10^{-8} t$	0.999
		$w_p^2 = 8.90 \times 10^{-8} t$	0.997
		$x^2 = -3.44 \times 10^{-8} + 3.67 \times 10^{-8} t^{1/2} + 4.64 \times 10^{-9} t$	
55	500	$w_f^2 = 1.16 \times 10^{-8} + 7.02 \times 10^{-7} t$	0.999
		$w_p^2 = 7.07 \times 10^{-7} t$	0.977
		$x^2 = 1.03 \times 10^{-9} + 6.23 \times 10^{-8} t$	
55	575	$w_f^2 = -1.78 \times 10^{-5} + 2.02 \times 10^{-5} t^{1/2} + 2.94 \times 10^{-6} t$	1.0
		$w_p^2 = 4.59 \times 10^{-6} t$	0.986
		$x^2 = -1.58 \times 10^{-6} + 1.79 \times 10^{-6} t^{1/2} + 2.61 \times 10^{-7} t$	
55	650	$w_f^2 = -3.77 \times 10^{-4} + 4.88 \times 10^{-4} t^{1/2} + 3.48 \times 10^{-5} t$	0.998
		$w_p^2 = 8.99 \times 10^{-5} t$	0.946
		$x^2 = -3.35 \times 10^{-5} + 4.33 \times 10^{-5} t^{1/2} + 3.09 \times 10^{-6} t$	

[a] The three equations at each temperature correspond to best fit of the experimental data, parabolic model, and scale thickness.
[b] No measurable weight gain was observed for this specimen.
The last column indicates the degree of fit obtained from the regression analysis of data.

density, which is 3.357 g cm^{-3} (or mg mm^{-3}) for V_2O_5, and is provided for obvious practical reasons — to allow ready estimation of the scale thickness, x, for any desired time at each temperature. The coefficient of time (t) in each equation is the rate constant (denoted by k in general, and by k_f, k_p, or k_x, depending on the models described in Table 2) at the corresponding temperature with the units as indicated. No measurable weight gain was observed in the 55 alloy oxidized at 300°C.

The TGA data for the 44 and 55 alloys are presented in Fig. 3 as plots of weight gain versus time. In these plots, the lines represent the oxidation models that best fit the experimental data, which are shown as circles for the 44 samples and as squares for the 55 samples. The results show that in both alloys, oxidation (scale growth) occurs according to a non-linear growth rate law, and that the rate of oxidation decreases with time, indicating a protective oxide scale. Together with the lack of spalling of the scale, these results provide evidence that V_2O_5 forms as a non-porous and tenacious oxide on the surface of 44 and 55 alloys in the temperature range of 350–650°C. As can be seen from the plots in Fig. 3, oxidation rate increased with increasing temperature. As expected, the temperature-dependence of the rate constant was Arrhenius in nature, and the data for both alloys fitted well an equation of the form

$$k = k_o \exp[-Q_{ox}/(RT)], \quad (1)$$

where k is the rate constant (k_f, k_p, or k_x), k_o is the pre-exponential constant, Q_{ox} is the activation energy for the oxidation process, and R and T are the gas constant and absolute temperature, respectively. The Arrhenius plots of k_f versus reciprocal temperature for the 44 and 55 alloys are shown in Fig. 4. It can be seen from this figure that there is little difference between the rate constants at a given temperature and the slope of the line for the two alloys, with those for the 44 slightly higher. While the oxide that forms on both alloys is predominantly V_2O_5, the slightly higher oxidation resistance of the 55 alloy may be attributable to its slightly higher substitutional alloying

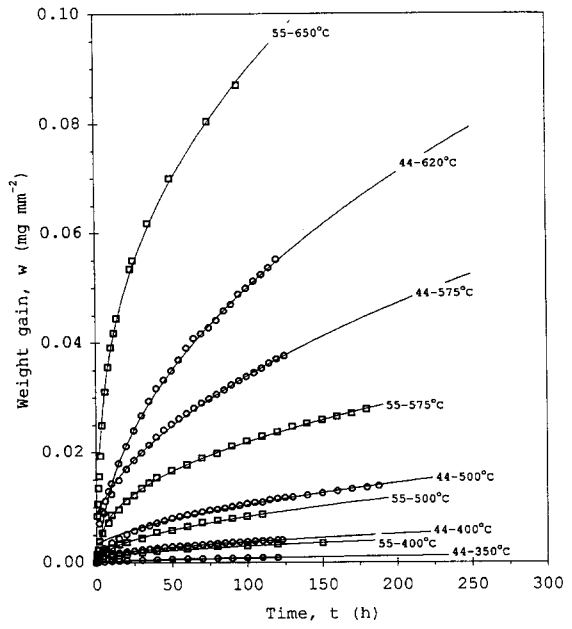

Fig. 3. Variation of weight gain with time in air for 44 and 55 alloys. At each temperature, data points are from TGA experiments, and line represents model that best describes oxidation behavior of alloy.

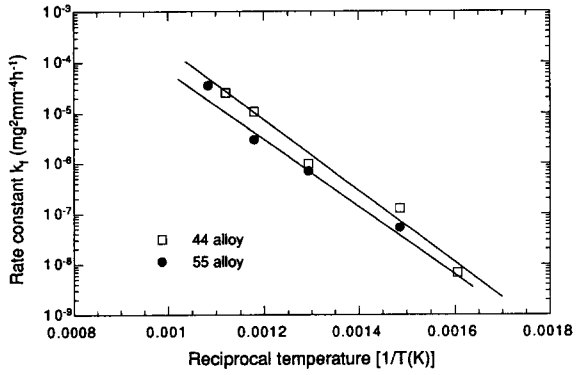

Fig. 4. Arrhenius plots of oxidation rate constants for 44 and 55 alloys exposed to air at temperatures of up to 650°C.

content (see Table 1), especially Ti, which is known to trap oxygen and slow its diffusion in the matrix. This may also be due to the larger average grain size of the 55 alloy, which means a smaller grain boundary area. The activation energies for the air-oxidation process as determined from the k_f values in Fig. 4 were about 135 kJ/mol for the 44 alloy and 130 kJ/mol for the 55 alloy.

Based on the work of Wagner [33], Wach proposed a relationship to facilitate determination of the numerical

Table 3
Rate constants for oxidation of V and V–4 wt% Cr–4 wt% Ti (44) and V–5 wt% Cr–5 wt% Ti (55) alloys, and calculated values of diffusion coefficients, and activation energies of diffusion of oxygen in V_2O_5 under conditions indicated

Alloy [a]	T (°C)	pO_2 (Torr)	Oxide	Rate constant [b] ($mg^2\ mm^{-4}\ h^{-1}$) ($k \times 10^9$)	D [c] ($m^2\ h^{-1}$) ($D \times 10^{15}$)	Q_D [d] (kJ mol^{-1})
V	450	760	V_2O_5	201	497	174.4
V	500	7.6	VO_2	367	56.9	193.6
V	500	760	V_2O_5	2740	630	164.7
V	550	3	VO_2	918	142	202.7
V	550	9	VO_2	1920	297	194.3
V	550	36	VO_2	2100	338	192.8
V	550	760	V_2O_5	8530	1980	172.0
V	600	1	VO_2	2880	446	209.7
V	600	4	VO_2	6160	954	200.1
V	600	7.6	VO_2	7420	1150	197.8
V	600	760	V_2O_5	19 600	4500	179.9
V	650	0.76	VO_2	4790	742	224.5
V	650	7.6	VO_2	10 800	1680	213.1
44	350	160	V_2O_5	6.76	1.6	165.6
44	400	160	V_2O_5	128	29.3	161.0
44	500	160	V_2O_5	982	225	178.0
44	575	160	V_2O_5	10 700	2460	179.0
44	620	160	V_2O_5	25 400	5830	184.0
55	400	160	V_2O_5	52.3	12	168.4
55	500	160	V_2O_5	702	161	181.7
55	575	160	V_2O_5	2940	673	194.0
55	650	160	V_2O_5	34 780	7980	191.0

[a] Data on V are from Ref. [27], and those on 44 and 55 are from this study.
[b] Rate coefficients for V are coefficients of time in a parabolic oxide growth rate model, and those for 44 and 55 alloys are coefficients of time in oxidation models that best fit the data in Table 2.
[c] Calculated from Eq. (2) with rate constants in Table 2.
[d] Calculated from Eq. (3) with D values in this table.

Table 4
Results of air-oxidation experiments at 500°C for various times

Alloy oxidation time (h)	Oxide thickness (μm)		Diffusion distance (μm)		Grain size [e] (μm)	Maximum aspect ratio
	measured [a]	calculated [b]	VHN [c]	SIMS [d]		
44-annealed	–	–	–	–	25	3.8
44-24	1.9	1.8	30	–	22	3.8
44-260	5.4	4.9	100	–	25	3.9
44-600	7.8	7.3	112	–	26	4.3
44-1050	10.2	9.6	–	–	26	4.3
44-2100	14.8	13.6	–	–	27	3.9
55-annealed	–	–	–	–	36	3.8
55-24	1.2	1.2	< 25	20	39	3.3
55-260	4.6	4.1	57	60	38	3.5
55-600	6.5	6.1	100	–	37	3.4
55-1050	8.4	7.9	105	110	35	4.1
55-2100	12.6	11.5	135	160	37	3.8

[a] Measured by metallographic techniques.
[b] Calculated with model that best fit experimental data in Table 2.
[c] Determined from Vickers microhardness measurements using 25 g weight.
[d] Determined from oxygen line profile obtained by secondary-ion mass spectroscopy.
[e] Error in grain-size values was about ±4 μm.

value of the diffusion coefficient, D, from a single value of the parabolic rate constant k_p as [34]

$$k_p = 2 D_i W_i^2 \rho^2, \tag{2}$$

where D_i is the diffusion coefficient of the diffusant i, W_i is its mass fraction in the oxide scale that forms, and ρ is the density of the oxide in the scale. For V_2O_5, $W_i = 0.4398$ and $\rho = 3.357$ g/cm^3. Based on the Wert–Zener–Le Claire equation, Wach showed that the activation energy for diffusion, Q_D, can be estimated from a single value of D at a temperature T as follows [34]:

$$D = D_\theta \exp\left[Q_D/R(1/\theta - 1/T)\right], \tag{3}$$

with D_θ and θ, which are the characteristic constants of the diffusant, given as

$$D_\theta = h/(4\pi m), \tag{4a}$$

$$\theta = h\nu/k_B, \tag{4b}$$

where h and k_B are the Planck's and Boltzmann's constants, respectively; m is the mass per atom of the diffusing species; and n is its vibrational frequency. D_θ for oxygen, as formulated from the minimum value of the uncertainty principle above, equals 1.99×10^{-9} m^2/s. Also for oxygen, θ equals 2050 K if an ν value of 4.27×10^{13} Hz is used. The values of the rate constants for V_2O_5, and the values of D calculated from Eq. (2) and Q_D calculated from Eq. (3) are listed in Table 3 for both the 44 and 55 alloys.

Also included in the table are the 450–600°C data from the work of Mukherjee and Wach on the oxidation of V [27]. In all V samples, only V_2O_5 formed at 760 Torr (1 atm) oxygen pressure, and the oxide that formed at an oxygen partial pressure of 36 Torr and below was VO_2. No data were available for V at the pressures used in this study (160 Torr, or 0.21 atm oxygen) for the 44 and 55 alloys, all of which formed V_2O_5. In the V samples above 450°C, the rate constant, k_p, for V_2O_5 is consistently higher than that for VO_2 at each temperature, accompanied

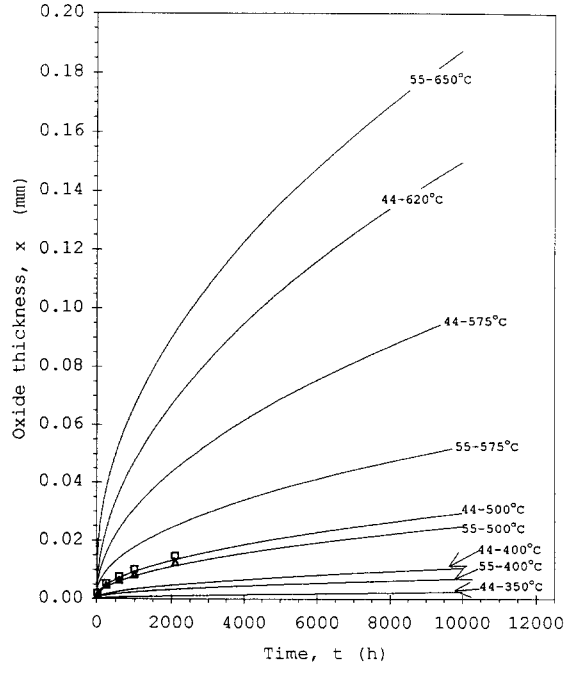

Fig. 5. Model-based plots of oxide thickness versus time, extrapolated to 10000 h with metallographically measured scale thicknesses shown as data points.

by a higher diffusion coefficient and a lower activation energy for diffusion of oxygen in the oxide. Also in V, at lower oxygen pressures ($pO_2 \leq 36$ Torr), the increases in k and D with increasing pressure are rather significant and are accompanied by little change in Q_D. As will be noted from the results of this study in Table 3, the k and D values are measurably higher for the 44 alloys than for the 55 alloys, and there is little difference in their Q_D values. However, the k and D values for both alloys are lower than the corresponding values for unalloyed V regardless of the oxygen pressure and especially above 500°C.

The lower surface oxidation rate in the 44 and 55 alloys than in unalloyed V may be attributed to increasing Ti content, which slows the diffusion of oxygen into the matrix and thus decreases the rate of V_2O_5 formation. The activation energies of diffusion of oxygen in V_2O_5 in Table 3 average to ≈ 173 kJ/mol for V, 174 kJ/mol for 44 alloy, and 184 kJ/mol for 55 alloy, and are all within 10% of one another. These values are greater than the activation energies of oxidation of the 44 and 55 alloys as calculated from the temperature dependence of rate constants (see Fig. 4 and Eq. (3)). This may be attributed to the component of the energy associated with the dissociation and adsorption of oxygen, which is endothermic [27]. Nevertheless, the results based on the decreasing rate with increasing time clearly show that oxidation of the 44 and 55 alloys in air appears to be controlled by the diffusion of oxygen in V_2O_5 in the temperature range of 300–650°C.

Table 4 shows the results of the air oxidation experiments at 500°C for times of 24 to ≈ 2100 h. The oxide scale thicknesses in column 2 were obtained from metallographic measurements and those in column 3 were calculated using the best-fit oxidation models developed from the TGA results (see Table 2). Plots of these models in the form of oxide scale thickness (x) versus time are shown in Fig. 5 for each of the 44 and 55 TGA samples, as extrapolated to 10000 h. Also included in the figure as data points are the experimentally measured scale thicknesses for both alloys at 500°C. It is evident from this figure and from columns 2 and 3 in Table 4 that there is

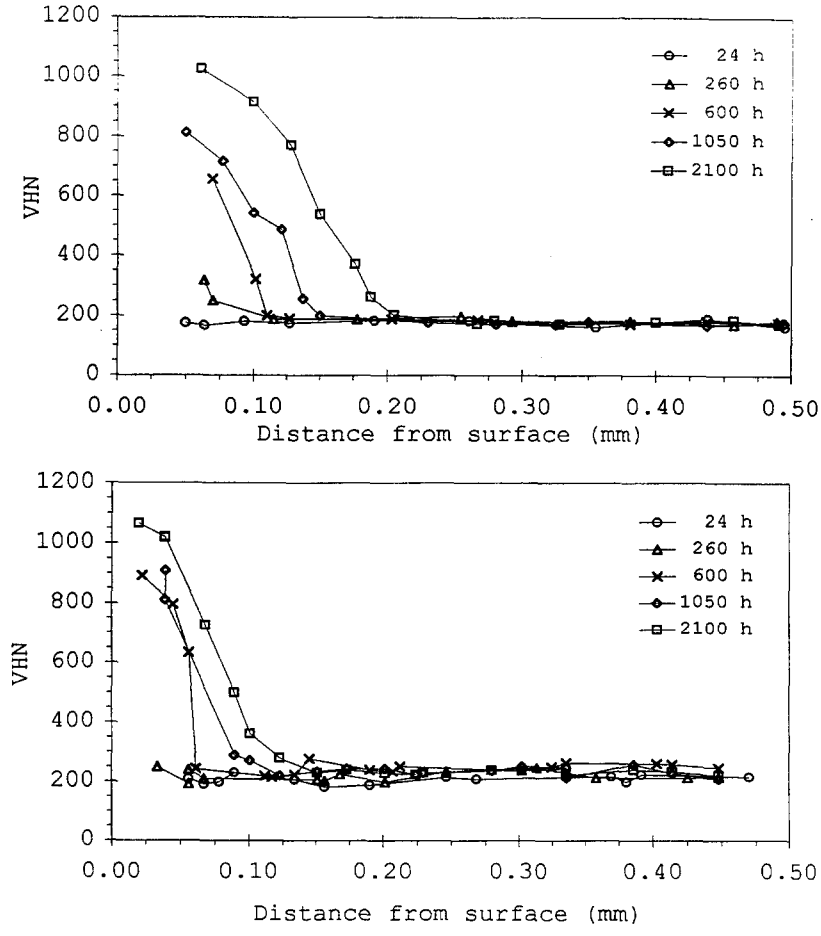

Fig. 6. Variation with time of Vickers hardness profile of cross section in thickness direction of air-oxidized (top) 44 alloy, and (bottom) 55 alloy.

good agreement between the scale thicknesses calculated from the models and those measured experimentally. The calculated values are within 10% of the measured values, indicating that the models developed from the TGA results describe the oxidation behavior of the 44 and 55 alloys rather well at 500°C. This should also be true for those at the other temperatures studied in this work because all such experiments in the temperature range of 300–650°C were carried out with the same apparatuses under similar conditions except for temperature.

The oxygen diffusion distances in columns 4 and 5 were estimated from, respectively, Vickers (VHN) microhardness profiles and secondary-ion mass spectroscopy (SIMS) oxygen-line profiles across the thickness of the specimens. Each value represents the approximate distance from the sample surface at which the profile stopped descending or leveled off. These were determined from plots of VHN versus distance along the sample thickness as shown in Fig. 6(a), (b) for the 44 and 55 samples, respectively. The relatively good agreement between the values obtained from VHN and SIMS-oxygen profiles in Table 4 indicates that the hardness change across the thickness of a sample was due predominantly to variation in oxygen content.

Columns 6 and 7 in Table 4 list, respectively, average grain size and maximum aspect ratio of the annealed and air-oxidized 44 and 55 samples. Photomicrographs in Fig. 7 show the grain structure of the cross-sections of the specimens, which were cold-rolled, vacuum-annealed at 1050°C for 1 h, air-oxidized at 575°C for up to 180 h, and air-oxidized at 500°C for ≈ 2100 h. Examination of grain-size data and photomicrographs reveals that the grains of the 44 samples were smaller than those of the 55 samples in a given condition. The grains were non-uniform in size throughout the specimens, but were somewhat equiaxed, and the maximum aspect ratio of the grains in all the samples exposed to elevated temperatures was 3 to 4. There was no evidence of grain growth or change in grain morphology after ≈ 2100 h at 500°C. Similar observations on grain size and shape were made in the TGA samples

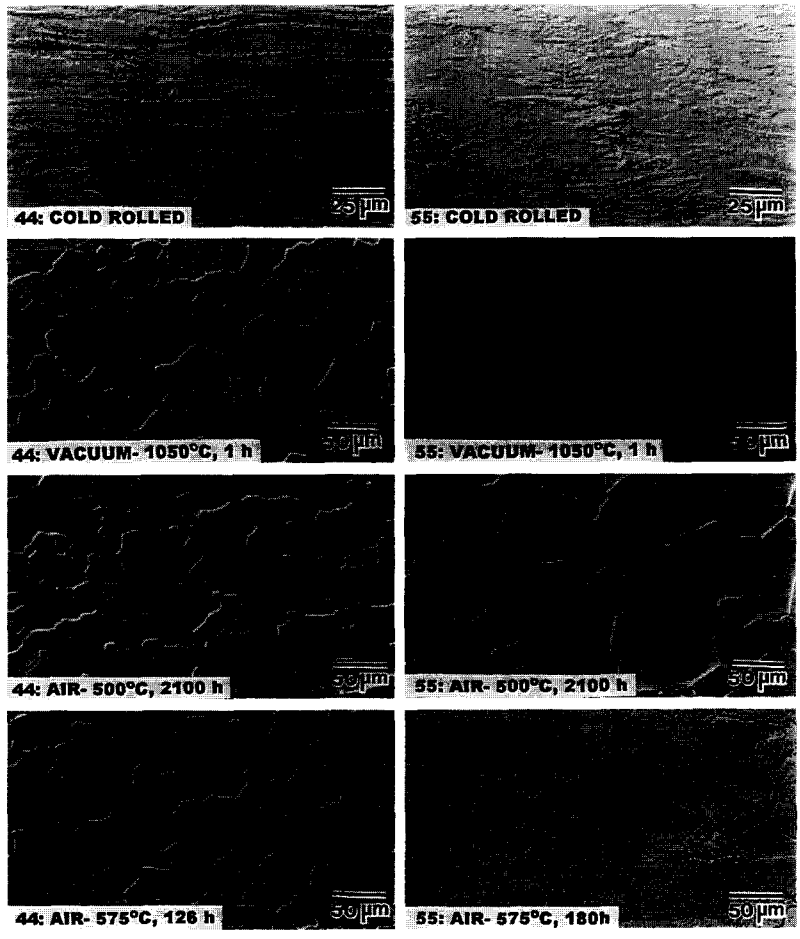

Fig. 7. Optical photomicrographs of 44 and 55 alloy sheets in different conditions as indicated. As-etched, differential interference contrast.

heated to as high as 575°C for up to ≈ 200 h, as seen also from Fig. 7. The grain size and morphology of heat treated samples in this figure are typical of all the others examined in this study. The stability of the grain size of these alloys at elevated temperatures may be due to the presence of complex precipitates of Ti(O, N, C) along the grain boundaries, reported in the literature [35].

Oxidation rate constants, and data for diffusion of O in V and its alloys with Cr and/or Ti and in V_2O_5 are tabulated in Table 5 (data sources are Refs. [36,37]). The rate constants for the 44 and 55 alloys in column 2 were obtained from the variation of the measured oxide scale thickness with time as presented in Table 4, and those in column 3 are from the oxidation models developed with the TGA results (see Table 2 or 3). Data for oxygen diffusion in V and its alloys, as well as in the oxides that form on them are given in columns 4–7 of Table 5 together with the data for the 44 and 55 alloys from this work and data for others from the literature as indicated. The diffusion coefficients, D, of O in the 44 and 55 alloys were determined from the oxygen diffusion distance–time data in Table 4, assuming one-dimensional diffusion, hence

$$x \propto (Dt)^{1/2}, \tag{5}$$

which should be valid on the basis of the geometry of the samples used in this study. Using these diffusion coefficients, we calculated the activation energies of diffusion of oxygen in these alloys from Eq. (3). The good agreement between the rate constant calculated from the measured data and that from the model for both the 44 and 55 alloys indicates, again, that the models developed in this study describes the oxidation behavior of these alloys rather well. The diffusion coefficient was greater for oxygen diffusion in the 44 alloy than in the 55 alloy, and their magnitudes were between those in V-5Cr and V-5Ti alloys. The activation energy of oxygen diffusion was, as expected, higher for the 55 alloy than for the 44 alloy. However, the activation energies of oxygen diffusion in either alloy were greater than those in unalloyed V and in the V-5Cr alloy, but considerably lower than that in V-5Ti alloy.

These trends may be attributed to the binding or trapping of O by the Ti atoms that are in solid solution. On the other hand, the activation energies for the diffusion of oxygen in the oxides that formed on V and on the 44 and 55 alloys were within 10% of one another. This would strongly indicate that the oxides that formed on these materials were similar in nature, namely V_2O_5.

4. Conclusions

A study was conducted to determine and compare the air-oxidation behavior of V–4Cr–4Ti (44) and V–5Cr–5Ti (55) alloys in the temperature range of 300–650°C. From the results obtained, the following conclusions are drawn:

- The oxide that formed on either alloy was predominantly V_2O_5 with some VO_2 and/or a complex (V, Cr, Ti) oxide possibly also present.
- Oxide scales on both alloys were continuous and tenacious, and the oxidation kinetics followed a parabolic or a nearly parabolic non-linear growth rate law.
- 55 alloys were consistently more oxidation-resistant than the 44 alloys, and the difference in their oxidation resistance increased with increasing temperature above 500°C.
- Oxygen diffusion was faster in the 44 alloy than in the 55 alloy. However, the activation energies of diffusion of oxygen in both alloys were within 5% of one another.
- The microstructures of both alloys were quite stable, because no measurable grain growth was observed in either after 2100 h at 500°C or after ≈ 200 h at 650°C.

Table 5
Air-oxidation rate constants, and for oxygen diffusion in V and some of its alloys with Cr and/or Ti and in V_2O_5

Alloy	Rate constant at 500°C ($k \times 10^9$) ($mg^2\ mm^{-4}\ h^{-1}$)		Diffusion coefficient at 500°C ($D \times 10^{15}$) ($m^2\ h^{-1}$)		Activation energy of diffusion (Q) ($kJ\ mol^{-1}$)	
	tabs [a]	TGA [b]	metal/alloy [c]	oxide [d]	alloy	oxide
V	–	2740	40680 [f]	630	123 [f]	165 [e]
V–5Cr	–	–	12096 [g]	–	111 [g]	–
V–5Ti	–	–	2747 [g]	–	172 [g]	–
44	1100	982	23760	225	130 [e]	178 [e]
55	830	702	9720	161	140 [e]	182 [e]

[a] Parabolic rate constant calculated from variation of measured oxide scale thickness with time in Table 4.
[b] Rate constants as given and described in Table 3.
[c] Calculated at 500°C from oxygen diffusion distance into 44 and 55 alloys as provided in Table 4.
[d] Calculated from oxide scale thickness, and values are as given and described in Table 3.
[e] Calculated from Eq. (3) using the D values in columns 4 and 5 of this table. The values for the alloys are based on microhardness profile data and those for the oxides are based on scale thickness data.
[f] From Ref. [36].
[g] From Ref. [37].

Acknowledgements

This work was supported by the US Department of Energy, Office of Fusion Energy Research, under Contract W-31-109-Eng-38. The assistance of D.L. Rink (Energy Technology Division, Argonne National Laboratory) in the metallography and oxidation experiments is gratefully acknowledged. Special thanks are due to Todd E. Leonhardt (Materials Division, NASA Lewis Research Center) for his assistance in preparing some of the metallographic samples.

References

[1] W. Rostoker, A.S. Yamamoto and R.E. Riley, Trans. Am. Soc. Met. 48 (1956) 560.
[2] B.R. Bajala and R.S. Van Thyne, J. Less-Common Met. 3 (1961) 489.
[3] J. Wadsworth, T.G. Nieh and J.J. Stephens, Int. Mater. Rev. 33 (1988) 131.
[4] R.C. Hought and S.M. Grimes, in: Neutron Data of Structural Materials for Fast Reactors, ed. K.H. Bockhoff (Pergamon, New York, 1979) p. 312.
[5] A. Smith, R. McKnight and D. Smith, in: Neutron Data of Structural Materials for Fast Reactors, ed. K.H. Bockhoff (Pergamon, New York, 1979) p. 374.
[6] C.J. McHargue and J.L. Scott, Metall. Trans. 9A (1978) 151.
[7] T. Noda, F. Abe, H. Araki and M. Okada, J. Nucl. Mater. 155–157 (1988) 581.
[8] R. Santos, J. Nucl. Mater. 155–157 (1988) 589.
[9] G.J. Butterworth, K.A. McCarthy, G.R. Smolik and C.B.A. Forty, J. Nucl. Mater. 212–215 (1994) 667.
[10] F.L. Yaggee, E.R. Gilbert and J.W. Styles, J. Less-Common Met. 19 (1969) 39.
[11] D.L. Smith, B.A. Loomis and D.R. Diercks, J. Nucl. Mater. 135 (1985) 125.
[12] R.E. Gold and R. Bajaj, J. Nucl. Mater. 122&123 (1984) 759.
[13] B.A. Loomis, A.B. Hull and D.L. Smith, J. Nucl. Mater. 179–181 (1991) 148.
[14] B.A. Loomis and D.L. Smith, J. Nucl. Mater. 191–194 (1992) 84.
[15] H.M. Chung and D.L. Smith, J. Nucl. Mater. 191–194 (1992) 942.
[16] H.M. Chung, B.A. Loomis and D.L. Smith, ASTM-STP 1175 (American Society for Testing and Materials, Philadelphia, PA, 1993) pp. 1185–1200.
[17] H.M. Chung, B.A. Loomis and D.L. Smith, Plasma Dev. Oper. 3 (1994) 167.
[18] V.A. Evtikhin, I.E. Lyublinski, V.Yu. Pankratov and L.P Zavyalski, J. Nucl. Mater. 191–194 (1992) 924.
[19] W.A. Simpson, in: Fusion Reactor Materials, Semiannual Progress Report, DOE/ER 0313/16, Oak Ridge National Laboratory, Oak Ridge, TN (March 1994) p. 258.
[20] H.M. Chung, B.A. Loomis and D.L. Smith, Fusion Eng. Des. 29 (1995) 455.
[21] O. Kubaschewski and C.B. Alcock, Metallurgical Thermochemistry, 5th Ed. (Pergamon, Oxford, 1979).
[22] R.J. Lauf and C.J. Altstetter, Acta Metall. 27 (1979) 1157.
[23] D.F. Hasson and R.J. Arsenault, in: Treatise on Materials Science and Technology, ed. H. Herman, Vol. 1 (Academic Press, New York, 1972) p. 179.
[24] E.A. Gulbransen and K.F. Andrew, J. Electrochem. Soc. 97 (1950) 396.
[25] W.R. Price and J. Stringer, J. Less-Common Met. 8 (1965) 165.
[26] W.R. Price, S.J. Kennett and J. Stringer, J. Less-Common Met. 12 (1967) 318.
[27] A. Mukherjee and S.P. Wach, J. Less-Common Met. 92 (1983) 289.
[28] G. Salomonsen, N. Norman, O. Lonsjo and T.G. Finstad, J. Less-Common Met. 158 (1990) 251.
[29] T. Suzuki, T. Noda, N. Iwao, T. Kainuma and R. Watanabe, J. Nucl. Mater. 62 (1976) 205.
[30] G. Busch and A. Tobin, J. Nucl. Mater. 141–143 (1986) 599.
[31] D.R. Diercks and D.L Smith, J. Nucl. Mater. 141–143 (1986) 617.
[32] J.H. DeVan, J.R. Distefano and J.W. Hendricks, in: Fusion Reactor Materials, Semiannual Progress Report, DOE/ER 0313/17, Oak Ridge National Laboratory, Oak Ridge, TN (Sept. 1994) p. 240.
[33] C. Wagner, Z. Phys. Chem. Abt. B21 (1933) 25.
[34] S. Wach, Proc. 2nd Int. Conf. on Hydrogen in Metals, Paris, June 1977 (Pergamon, Oxford, 1978) Paper 1A1.
[35] M. Satou and H.M. Chung, in: Fusion Reactor Materials, Semiannual Progress Report, DOE/ER-0313/13, Oak Ridge National Laboratory, Oak Ridge, TN (1993) pp. 227–234.
[36] F.A. Schmidt and J.C. Warner, J. Less-Common Met. 26 (1972) 325.
[37] H. Nakajima, S. Nayata, H. Matsui and S. Yamaguchi, Philos. Mag. 67 (1993) 557.